Discovery of the FeO orange bands in the terrestrial night airglow spectrum obtained with OSIRIS on the Odin spacecraft

W. F. J. Evans,[1,2] R. L. Gattinger,[3] T. G. Slanger,[4] D. V. Saran,[4] D. A. Degenstein,[3] and E. J. Llewellyn[3]

Received 31 August 2010; revised 4 October 2010; accepted 13 October 2010; published 20 November 2010.

[1] An unidentified pseudo-continuum in the 600 nm region is observed in the upper mesosphere with the limb-scanning OSIRIS imaging spectrograph on-board the Odin spacecraft. Averages of low latitude spectra at a series of tangent limb altitudes from 75 to 105 km are assembled and matched with synthetic spectra of the known night airglow emission band systems to isolate the underlying airglow continuum. The upper limit of the NO + O → NO_2* air afterglow continuum component in the observed 600 nm pseudo-continuum is estimated to be 5% at low latitudes. The spectral profile of the unidentified 600 nm residual airglow continuum is very similar to published laboratory measurements of the 'orange bands' of FeO. The volume emission rate altitude profile of this 600 nm airglow continuum, derived from averaged limb radiance profiles, is very similar in shape and in altitude to the concurrently observed Na vertical profile suggesting related source mechanisms. **Citation:** Evans, W. F. J., R. L. Gattinger, T. G. Slanger, D. V. Saran, D. A. Degenstein, and E. J. Llewellyn (2010), Discovery of the FeO orange bands in the terrestrial night airglow spectrum obtained with OSIRIS on the Odin spacecraft, *Geophys. Res. Lett.*, *37*, L22105, doi:10.1029/2010GL045310.

1. Introduction

[2] The terrestrial night airglow spectrum has been studied quantitatively for more than a century. Early ground-based studies include the first measurement of the wavelength of the mysterious 'green line' by *Ångström* [1869], reported as 5567 Ångströms. *McLennan and Shrum* [1925] identified the source of the green emission as a transition from the OI metastable $^1S_0$ state to the $^1D_2$ state. *Barbier et al.* [1951] analyzed dual wavelength observations of the green emission to establish an accurate background correction and confirmed the presence of an underlying terrestrial based continuum, in addition to the star background and zodiacal light inherent in ground-based observations. *Sternberg and Ingham* [1972] reviewed the previous night airglow continuum observations and, after removing the non-terrestrial sources, calculated the absolute continuum differential brightness at a series of wavelengths in the visible and near infrared from their spectrometric observations, conducted at Observatoire de Haute Provence at approximately 44° North. They found the continuum peaks around 600 nm and noted its similarity to the NO + O → NO_2* chemiluminescent air afterglow spectrum.

[3] A number of observations of the NO_2* air afterglow emission have been made at higher latitudes. In a series of rocket flights into auroral displays *Sharp* [1978] observed the NO_2* air afterglow emission peaking between 100 and 110 km. *Witt et al.* [1979, 1981] observed the NO_2* air afterglow in the auroral zone but with no aurora in the field of view. During the ETON rocket campaign, conducted at approximately 57° North, *McDade et al.* [1986] observed the maximum brightness in the vertical profile of the 540 nm night airglow continuum at approximately 98 km along with a fainter second layer at approximately 90 km. Using spectrometric limb observations from the space shuttle STS-37 mission *Mende et al.* [1993] observed a green continuum at 103 km ± 2 km at low latitudes.

[4] *Bates* [1993] provided a critical analysis of the proposed night airglow continuum source mechanisms and suggested that the NO_2* air afterglow contributes only a fairly small fraction of the total. From a series of observations that covered the complete southern hemisphere *Gattinger et al.* [2010] concluded that the NO_2* night airglow emission is much brighter at polar latitudes than at low latitudes. Accordingly, attempts to detect faint emissions in the night airglow spectrum are more likely to succeed at lower latitudes. The chemiluminescent NO + O_3 → NO_2* + O_2 reaction also produces emission in the 600 nm region [*Clough and Thrush*, 1967] and can potentially contribute to the airglow signal, although *Bates* [1993] concluded that for this mechanism "the contribution to the nightglow is inappreciable".

[5] Recently, *Cosby and Slanger* [2007] assembled a night sky spectrum from the echelle spectrograph and imager (ESI) on the Keck II telescope on Mauna Kea, approximately 20° north latitude. The spectrum shows a structured continuum in the 550 to 650 nm region that does not match the spectral shape of the chemiluminescent NO + O → NO_2* emission. *Jenniskens et al.* [2000] observed a similar spectrally structured continuum in the 550 to 650 nm region in a Leonid meteor persistent train and noted the spectral match with the laboratory spectrum of the FeO 'orange bands'. The primary focus of the current analysis is this 550 to 650 nm structured continuum observed in the terrestrial night airglow spectrum at low latitudes. The observations, made with the OSIRIS space-borne limb-scanning spectrograph, and the spectral isolation procedures, are discussed in the

[1]NorthWest Research Associates, Inc., Redmond, Washington, USA.
[2]Centre for Research in Earth and Space Science, York University, Toronto, Ontario, Canada.
[3]ISAS, Department of Physics and Engineering Physics, University of Saskatchewan, Saskatoon, Saskatchewan, Canada.
[4]Molecular Physics Laboratory, SRI International, Menlo Park, California, USA.

0094-8276/10/2010GL045310

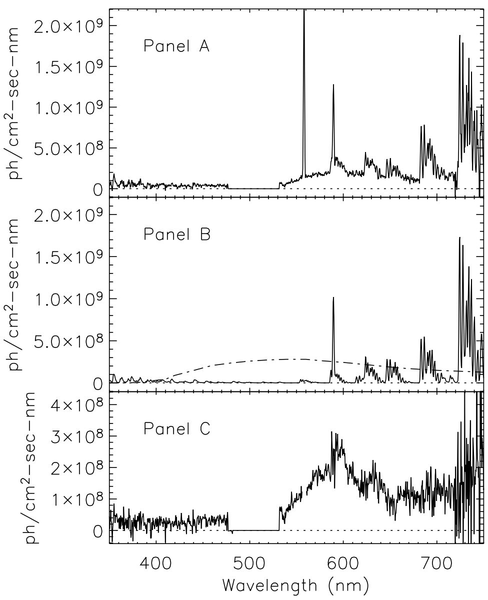

Figure 1. (a) The 350 nm to 750 nm observed night airglow limb radiance spectrum averaged from 80 to 92 km tangent limb altitudes. Data are from five 24 hr observing periods between 20 April 2003 and 27 May 2003, between the Equator and 40° South. Observations in the 480 nm to 530 nm OSIRIS order sorter region are omitted. (b) Solid: Matching synthetic spectra of the O_2 Herzberg, Chamberlain and Atmospheric band systems, the OH vibration-rotation system and the Na doublet. DotDash: Estimated upper limit (scaled up by ten times) of the NO + O → NO_2* component. (c) The difference signal, Figure 1a spectrum minus Figure 1b spectrum, with expanded vertical scale. The data gap over the 480 to 530 nm region in the observed OSIRIS spectrum is due to the order sorter.

following sections. The volume emission rate (VER) altitude profile of the structured continuum is compared with other emission features present in the observed spectrum. A brief discussion of possible source mechanisms for the 550 to 650 nm continuum is also presented.

2. Instrumentation and Observations

[6] The observations reported here are from the Optical Spectrograph and Infra-Red Imager System (OSIRIS) [*Llewellyn et al.*, 2004] on the Odin spacecraft [*Murtagh et al.*, 2002]. The Odin spacecraft was launched on 20 February 2001 into a circular Sun-synchronous orbit, ascending node 1800 Local Time, orbit inclination 97.8°, and altitude 620 km. In aeronomy mode the OSIRIS field of view is scanned vertically across the tangent limb with a vertical field of view of 1 km, a scanning rate of approximately 0.75 km s^{-1} and exposure times typically 2 s in the upper mesosphere and lower thermosphere. Absolute pointing knowledge at the limb tangent point is known to better than one-half kilometer. As OSIRIS has a spectral imaging CCD detector, all emissions in the 275 to 815 nm wavelength range are exposed simultaneously facilitating the accurate determination of relative spectral intensities. The spectral resolution is approximately 0.90 nm.

[7] To obtain reliable emission ratios that are separated widely in wavelength, an accurate relative spectral calibration of the OSIRIS instrument is essential. Pre-launch calibrations used NIST calibrated standard lamps followed by on-orbit astronomical observations to refine the calibration. The resulting absolute calibration error is estimated to be ±10% and the precision approximately 5%. During the mission, response changes are monitored by a comparison between the observed on-orbit daytime limb scatter spectra and simulations using the SASKTRAN three-dimensional radiative transfer model described by *Bourassa et al.* [2008]. Multiple Rayleigh molecular scatter, Mie aerosol scatter, molecular atmospheric extinction and Lambertian ground albedo effects are included in the model. Using auroral emissions observed by OSIRIS at multiple wavelengths and with common upper states, *Gattinger et al.* [2009] confirmed the accurate relative calibration in the ultraviolet and blue regions.

[8] Spectra from individual limb scans are analyzed over the 75 to 105 km limb tangent altitude range. For each limb scan a slowly changing CCD dark pattern is determined from the exposures in the 105 to 110 km tangent altitude range and subtracted from the observed tangent limb spectra. This background subtraction procedure automatically removes any non-terrestrial emission sources. Only those spectra for which the solar zenith angle was greater than 101° were considered in the analysis to exclude the effects of scattered solar radiation.

[9] An averaged airglow spectrum from 350 to 750 nm, limb altitude range from 80 to 92 km, is shown in Figure 1a. The spectrum is from latitudes between the Equator and 40° south over five 24 hr observing periods between 20 April 2003 and 27 May 2003. Latitudes poleward of 40° have been excluded in order to minimize the contribution of the chemiluminescent NO + O → NO_2* reaction arising from enhanced NO in the dark polar regions [*Gattinger et al.*, 2010].

[10] The obvious airglow features are the OI (^1S – ^1D) atomic line at 557.7 nm, the Na emission doublet centred on 589.3 nm and a number of OH vibration-rotation bands. The weak emissions in the ultraviolet region are from the Herzberg and Chamberlain band systems. Faint emission features arising from the $O_2(b^1\Sigma_g^+ - X^3\Sigma_g^-)$ band system are present in the 710 nm spectral region. In addition to these known emissions there appears to be an unidentified 'continuum' feature in the 600 nm region. Procedures for spectrally isolating this underlying continuum are described in the next section.

3. Spectral Analysis

[11] Model spectra of band systems known to be present in the night airglow were generated for comparison with the observed spectral features in Figure 1a. Each of the model spectra were convolved with the approximately 0.90 nm OSIRIS instrumental function before scaling to the observed spectrum. For the ultraviolet and blue spectral regions the O_2 Herzberg and Chamberlain band model is from the tabulations by *Cosby et al.* [2006]. The model spectrum was scaled by comparison with the observed OSIRIS spectrum over the 350 to 400 nm region. For the visible and near infrared regions synthetic spectra of the OH Meinel bands were generated using the ground-based relative band

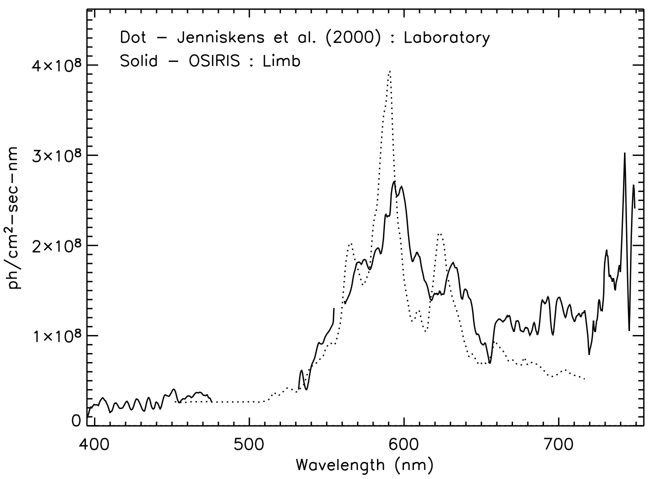

Figure 2. The difference spectrum from Figure 1c, arbitrarily smoothed to improve presentation, compared with a scaled laboratory spectrum of the FeO orange bands.

intensities observed by *Cosby and Slanger* [2007]. Following the analysis by *French et al.* [2000] the OH line strengths given by *Langhoff et al.* [1986] were assumed. The model OH band system was scaled to the OSIRIS OH observations by using the relatively bright OH 8-3 band at 730 nm. This resulted in a satisfactory match for the OH bands in the 530 to 720 nm region, except for the OH 7-2 band at 680 nm. In the ground-based observations this band is partially absorbed by the O_2 ($b^1\Sigma_g^+$-$X^3\Sigma_g^-$) 1-0 band in the lower atmosphere, thereby affecting the measured brightness of the band. For this band only an individual band scaling has been used based on the limb brightness observed by OSIRIS. Finally, small but detectable signals from the faint O_2 ($b^1\Sigma_g^+$-$X^3\Sigma_g^-$) 3-2 and 4-3 bands at 706 and 715 nm are used to scale the relative band intensities determined by *Slanger et al.* [2000] to the observed OSIRIS matching spectrum.

[12] The sum of the scaled model band systems is shown in Figure 1b. The Na doublet at 589.3 nm has also been included in the model sum. The difference between the observed spectrum in Figure 1a and the composite model spectrum in Figure 1b is shown in Figure 1c. It should be noted that the OI 557.7 nm emission feature is not included in the model spectrum and has been omitted in the following comparisons; in addition the ordinate scale in Figure 1c is increased by five times relative to Figure 1b. As a consequence of the increasing brightness of the OH bands towards longer wavelengths the noise level in the residual signal also increases. This residual spectrum in Figure 1c is tentatively classed as unexplained airglow emissions. There is an apparent uniform continuum in the 350 to 480 nm region and an obvious broad spectral feature centred on 590 nm. This 590 nm emission feature is the focus of the discussion below.

4. Discussion

[13] The calibrated airglow spectrum shown in Figure 1c is expanded in Figure 2 to show the 600 nm region in more detail. A 2.5 nm triangular smoothing function has been applied to the spectrum in order to improve the presentation clarity. It is relevant to estimate the extent to which this emission feature may contain a contribution from chemiluminescent NO_2* arising from NO + O → NO_2*. The NO_2* emission in the 90 km altitude region is generally limited to high latitudes where aurorally generated NO descends into the mesosphere in polar darkness [e.g., *Gattinger et al.*, 2010]. At low latitudes the NO generated through solar radiation is destroyed in the lower thermosphere under sunlit conditions [*Bailey et al.*, 2002]. The current observations are limited to latitudes equatorward of 40° in order to avoid the auroral NO_2* source. The upper limit of the NO + O contribution can be estimated from the difference in spectral shape between the residual night airglow continuum in Figure 2 and the mesospheric NO + O continuum observed by *Gattinger et al.* [2009]. From their tabulations the differential brightness at 470 nm is approximately 70% of that at 600 nm. The estimated maximum contribution from this mechanism, above the spectrally uniform emission in the 470 nm range in Figure 2, is approximately 1×10^7 photons cm^{-2} sec^{-1} nm^{-1}. The dot-dash line in Figure 1b shows the NO_2* chemiluminescent spectrum scaled up by a factor of ten based on this estimate. At 600 nm this corresponds to 1.4×10^7 photons cm^{-2} sec^{-1} nm^{-1}, which is approximately twenty times fainter than the observed differential brightness at 600 nm in Figure 2 indicating that NO + O → NO_2* is at most a minor source.

[14] The similarity of the observed OSIRIS spectral shape of this continuum is shown in Figure 2 where it is compared with a spectrum of the FeO emission bands obtained from a laboratory fast flow tube [*Jenniskens et al.*, 2000]. However, the spectral peaks in the laboratory spectrum are located at slightly shorter wavelengths relative to the peaks observed in the mesospheric observations; *Jenniskens et al.* [2000] have noted that "the relative heights and shapes of the three dominant FeO peaks may be somewhat different at low pressure when quenching is absent". From preliminary spectral simulations of the FeO bands a change in vibrational distribution, potentially caused by collisional quenching at the much higher laboratory pressures, can indeed cause the observed spectral differences.

[15] As a further investigation of the source of the 590 nm emission feature in Figure 2 the data have been compared with independent atmospheric measurements. For example, using LIDAR observations of Fe and Na at 40° north lati-

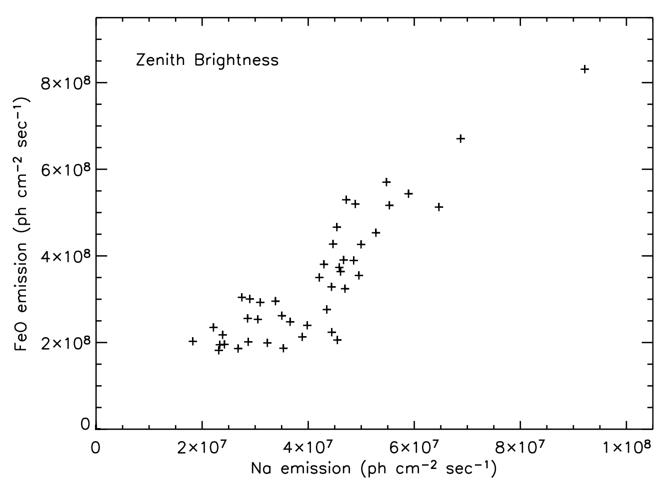

Figure 3. The correlation between the OSIRIS Na and FeO column emissions.

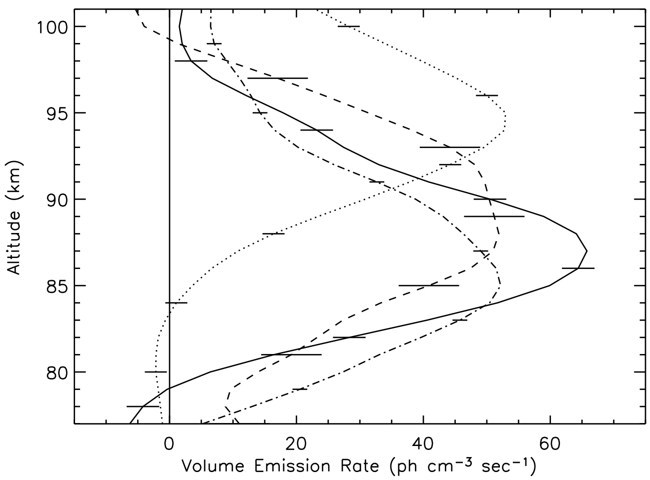

Figure 4. Scaled volume emission rate altitude profiles for the same dataset as in Figure 1. Solid – 600 nm continuum sum (564 to 680 nm)/10.0; short dash – Na/1.0; sotdash – OH 8-3 band/3.5; dot - 557.7/3.0.

tude *Kane and Gardner* [1993] reported the covariation of Fe and Na in both column abundance and layer height. From the OSIRIS observations the linear correlation between the Na and the FeO column emissions is approximately 0.9 (Figure 3), which also indicates a strong correlation.

[16] The LIDAR observations have also shown that the altitude of the Fe layer is approximately 4 km lower than the Na layer. The OSIRIS observed Na and FeO VER altitude profiles are shown in Figure 4. Noise estimates on the VER profiles are based on the observed signal variability of the 400 to 470 nm continuum in Figure 1c. From these OSIRIS observations the FeO emission layer centroid is approximately 3 km lower than the Na layer centroid, in approximate agreement with the LIDAR observations. The VER altitude profiles for the OI 557.7 nm emission and the OH 8-3 band, also included in Figure 4, are located at their typical layer altitudes so suggesting that the limb pointing is not in error.

[17] Since both sodium and iron oxide are excited in the laboratory by chemiluminescent reactions with ozone, and both metals have their source in meteorites, it is expected that FeO would be an emission feature in the night airglow. In addition the similarity of the altitude profile of the detected continuum emission with the altitude distribution of the Meinel OH band emission, shown in Figure 4, indicates that the feature should be due to chemiluminescent excitation involving ozone reactions. Indeed, the reaction cycle for FeO excitation is similar to the OH excitation cycle:

$$Fe + O_3 \rightarrow O_2 + FeO^*, \text{ followed by } FeO + O \rightarrow Fe + O_2.$$

Like atomic hydrogen the iron atom is recycled and catalytically enhances the conversion of odd oxygen into O_2. As noted above LIDAR measurements of atomic iron have shown that it is at the same altitude as the observed FeO feature. Thus the chemistry itself supports our belief that the emission feature is due to FeO. While it is possible that the chemiluminescent reaction $NO + O_3 \rightarrow NO_2^* + O_2$ could contribute to the observed emission it is at most a very minor contributor; this conclusion is based on previous measurements of the STRATOGLOW NO_2^* mechanism [*Evans and Shepherd*, 1996]. Thus we are confident in our conclusion that the emission is due to FeO.

[18] Following our discovery of the FeO 'orange bands' emission in the nightglow Slanger and co-workers (D. V. Saran et al., FeO emission in the mesosphere: Detectability and diurnal behavior, submitted to *Geophysical Research Letters*, 2010) have used data collected with both the ESI spectrograph on the Keck II telescope and the UVES spectrograph on the Very Large Telescope (VLT) in Chile to study the temporal variation of the FeO emission. Their results show that the FeO emission can exhibit dramatic temporal changes.

[19] **Acknowledgments.** This work was supported by the Canadian Space Agency and the Natural Sciences and Engineering Research Council (Canada). Odin is a Swedish-led satellite project funded jointly by Sweden (SNSB), Canada (CSA), France (CNES) and Finland (Tekes).

References

Ångström, A. J. (1869), Spektrum des nordlichts, *Ann. Phys.*, *137*, 161–163.

Bailey, S. M., C. A. Barth, and S. C. Solomon (2002), A model of nitric oxide in the lower thermosphere, *J. Geophys. Res.*, *107*(A8), 1205, doi:10.1029/2001JA000258.

Barbier, D., J. Dufay, and D. Williams (1951), Recherches sur l'émission de la raie verte de la lumière du Ciel nocturne, *Ann. Astrophys.*, *14*, 399–437.

Bates, D. R. (1993), Cause of terrestrial nightglow continuum, *Proc. R. Soc. London A*, *443*, 227–237, doi:10.1098/rspa.1993.0141.

Bourassa, A. E., D. A. Degenstein, and E. J. Llewellyn (2008), SASKTRAN: A spherical geometry radiative transfer code for efficient estimation of limb scattered sunlight, *J. Quant. Spectrosc. Radiat. Transf.*, *109*, 52–73, doi:10.1016/j.jqsrt.2007.07.007.

Clough, P. N., and B. A. Thrush (1967), Mechanism of chemiluminescent reactions between nitric oxide and ozone, *Trans. Faraday Soc.*, *63*, 915–925, doi:10.1039/tf9676300915.

Cosby, P. C., and T. G. Slanger (2007), OH spectroscopy and chemistry investigated with astronomical sky spectra, *Can. J. Phys.*, *85*, 77–99, doi:10.1139/P06-088.

Cosby, P. C., B. D. Sharpee, T. G. Slanger, D. L. Huestis, and R. W. Hanuschik (2006), High resolution terrestrial airglow emission line atlas from UVES/VLT: Positions, intensities, and identifications for 2808 lines at 314 to 1043 nm, *J. Geophys. Res.*, *111*, A12307, doi:10.1029/2006JA012023.

Evans, W. F. J., and G. G. Shepherd (1996), A new airglow layer in the stratosphere, *Geophys. Res. Lett.*, *23*, 3623–3626, doi:10.1029/96GL03333.

French, W. J. R., G. B. Burns, K. Finlayson, P. A. Greet, R. P. Lowe, and P. F. B. Williams (2000), Hydroxyl (6-2) airglow emission intensity ratios for rotational temperature determination, *Ann. Geophys.*, *18*, 1293–1303.

Gattinger, R. L., W. F. J. Evans, I. C. McDade, D. A. Degenstein, and E. J. Llewellyn (2009), Observation of the chemiluminescent $NO + O \rightarrow NO_2 + h\nu$ reaction in the upper mesospheric dark polar regions by OSIRIS on Odin, *Can. J. Phys.*, *87*, 925–932, doi:10.1139/P09-051.

Gattinger, R. L., et al. (2010), NO_2 air afterglow and O and NO densities from Odin-OSIRIS night and ACE-FTS sunset observations in the Antarctic MLT region, *J. Geophys. Res.*, *115*, D12301, doi:10.1029/2009JD013205.

Jenniskens, P., M. Lacey, B. J. Allan, D. E. Self, and J. M. C. Plane (2000), FeO "orange arc" emission detected in optical spectrum of Leonid persistent train, *Earth Moon Planets*, *82/83*, 429–438, doi:10.1023/A:1017079725808.

Kane, T. J., and C. S. Gardner (1993), Structure and seasonal variability of the nighttime mesospheric Fe layer at midlatitudes, *J. Geophys. Res.*, *98*, 16,875–16,886, doi:10.1029/93JD01225.

Langhoff, S. R., H.-J. Werner, and P. Rosmus (1986), Theoretical transition probabilities for the OH Meinel system, *J. Mol. Spectrosc.*, *118*, 507–529, doi:10.1016/0022-2852(86)90186-4.

Llewellyn, E. J., et al. (2004), The OSIRIS Instrument on the Odin Spacecraft, *Can. J. Phys.*, *82*, 411–422, doi:10.1139/p04-005.

McDade, I. C., E. J. Llewellyn, R. G. H. Greer, and D. P. Murtagh (1986), ETON 3: Altitude profiles of the nightglow continuum at green and near infrared wavelengths, *Planet. Space Sci.*, *34*, 801–810, doi:10.1016/0032-0633(86)90076-0.

McLennan, J. C., and G. M. Shrum (1925), On the origin of the auroral green line 5577 Angstrom, and other spectra associated with the Aurora Borealis, *Proc. R. Soc. London, Ser. A*, *108*, 501–512, doi:10.1098/rspa.1925.0088.

Mende, S. B., G. R. Swenson, S. P. Geller, R. A. Viereck, E. Murad, and C. P. Pike (1993), Limb view spectrum of the Earth's airglow, *J. Geophys. Res.*, *98*, 19,117–19,125, doi:10.1029/93JA02282.

Murtagh, D. P., et al. (2002), An overview of the Odin Atmospheric Mission, *Can. J. Phys.*, *80*, 309–319, doi:10.1139/p01-157.

Sharp, W. E. (1978), NO_2 continuum in aurora, *J. Geophys. Res.*, *83*, 4373–4376, doi:10.1029/JA083iA09p04373.

Slanger, T. G., P. C. Cosby, D. L. Huestis, and D. E. Osterbrock (2000), Vibrational level distribution of O_2 ($b^1\Sigma^+g$, v = 0-15) in the mesosphere and lower thermosphere region, *J. Geophys. Res.*, *105*, 20,557–20,564, doi:10.1029/2000JD900256.

Sternberg, J. R., and M. F. Ingham (1972), Observations of the airglow continuum, *Mon. Not. R. Astron. Soc.*, *159*, 1–20.

Witt, G., J. Stegman, B. H. Solheim, and E. J. Llewellyn (1979), A measurement of the $O_2(b^1\Sigma_g^+\text{-}X^3\Sigma_g^-)$ atmospheric band and the OI(^{1}S) green line in the nightglow, *Planet. Space Sci.*, *27*, 341–350, doi:10.1016/0032-0633(79)90111-9.

Witt, G., J. Rose, and E. J. Llewellyn (1981), The airglow continuum at high latitudes: An estimate of the NO concentration, *J. Geophys. Res.*, *86*, 623–628, doi:10.1029/JA086iA02p00623.

D. A. Degenstein, R. L. Gattinger, and E. J. Llewellyn, ISAS, Department of Physics and Engineering Physics, University of Saskatchewan, 116 Science Pl., Saskatoon, SK S7N 5E2, Canada.

W. F. J. Evans, NorthWest Research Associates, Inc., 4118 148th Ave. NE, Redmond, WA 98052, USA. (wayne.e@comcast.net)

D. V. Saran and T. G. Slanger, Molecular Physics Laboratory, SRI International, 333 Ravenswood Ave., Menlo Park, CA 94025, USA.